Article

Tl NMR Methods for the Characterization of Monovalent Cation Binding to Nucleic Acids

Michelle L. Gill, Scott A. Strobel, and J. Patrick Loria

J. Am. Chem. Soc., **2005**, 127 (47), 16723-16732• DOI: 10.1021/ja055358f • Publication Date (Web): 03 November 2005

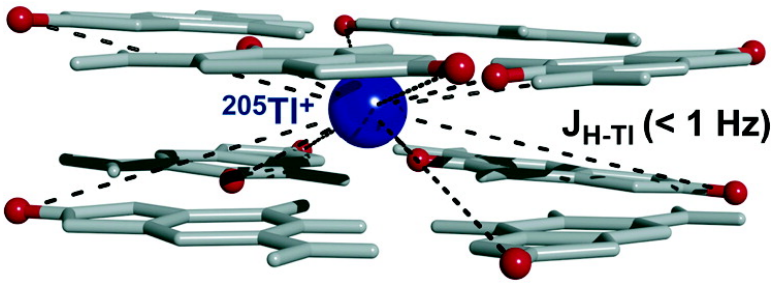

More About This Article

Additional resources and features associated with this article are available within the HTML version:

- Supporting Information
- Links to the 6 articles that cite this article, as of the time of this article download
- Access to high resolution figures
- Links to articles and content related to this article
- Copyright permission to reproduce figures and/or text from this article

View the Full Text HTML

J|A|C|S
ARTICLES
Published on Web 11/03/2005

^{205}Tl NMR Methods for the Characterization of Monovalent Cation Binding to Nucleic Acids

Michelle L. Gill,[†] Scott A. Strobel,[†,‡] and J. Patrick Loria*[,‡]

Contribution from the Department of Molecular Biophysics and Biochemistry, Yale University, New Haven, Connecticut 06520, and Department of Chemistry, Yale University, New Haven, Connecticut 06520

Received August 14, 2005; E-mail: patrick.loria@yale.edu

Abstract: Monovalent cations play an important role in many biological functions. The guanine rich sequence, $d(G_4T_4G_4)$, requires monovalent cations for formation of the G-quadruplex, $d(G_4T_4G_4)_2$. This requirement can be satisfied by thallium (Tl^+), a potassium (K^+) surrogate. To verify that the structure of $d(G_4T_4G_4)_2$ in the presence of Tl^+ is similar to the K^+-form of the G-quadruplex, the solution structure of the Tl^+-form of $d(G_4T_4G_4)_2$ was determined. The 10 lowest energy structures have an all atom RMSD of 0.76 ± 0.16 Å. Comparison of this structure to the identical G-quadruplex formed in the presence of K^+ validates the isomorphous nature of Tl^+ and K^+. Using a $^1H-^{205}Tl$ spin−echo difference experiment we show that, in the Tl^+-form of $d(G_4T_4G_4)_2$, small scalar couplings (<1 Hz) exist between ^{205}Tl and protons in the G-quadruplex. These data comprise the first $^1H-^{205}Tl$ scalar couplings observed in a biological system and have the potential to provide important constraints for structure determination. These experiments can be applied to any system in which the substituted Tl^+ cations are in slow exchange with the bulk ions in solution.

Introduction

Solution NMR plays a prominent role in structural biology. The power of this technique for determining macromolecular structures relies on establishing short range, interproton distances,[1] torsion angles,[2] and bond vector orientations.[3] These types of measurements are also useful in defining intermolecular interactions between macromolecules and small molecule ligands.[4] An important area of investigation that has not been as amenable to characterization by NMR is the study of interactions between inorganic cations and macromolecules. The difficulty in characterizing cation binding in solution arises primarily from the lack of metal ions with properties well suited for solution NMR. For the study of divalent cation binding sites by NMR, cadmium (^{113}Cd), a spin-$^1/_2$ nucleus, has been used as a surrogate for the biologically essential metals Ca^{2+} and Zn^{2+}.[5,6] To a lesser extent, mercury (^{199}Hg) NMR has also been used to study divalent cation sites.[7−9] These studies have enabled characterization of the interaction between divalent metal ions and their protein partners.[10−15] In addition, $^1H-M^{2+}$ heteronuclear experiments have been used to determine metal−ligand identity and binding site conformation and for the characterization of structural motifs in rubredoxin, metallothionein, superoxide dismutase, and the transcription factors GAL4 and LAC9.[7,8,11−17]

Likewise, monovalent cations are also essential for cellular function. Every major class of biomacromolecules including proteins,[18,19] nucleic acids,[20−24] phospholipids,[25−29] and carbohydrates[30−33] has a structural and/or functional requirement for monovalent cations. In nucleic acids, monovalent metal ions play structural and catalytic roles within the group I and II introns, RNaseP, and the ribosome.[23,34−36] The apparent specificity of these binding sites for monovalent cations implies a functional role warranting further investigation. Thus far, the most effective technique for high-resolution study of monovalent cations has been X-ray crystallography, often involving soaks

[†] Department of Molecular Biophysics and Biochemistry.
[‡] Department of Chemistry.

(1) Wuthrich, K. *NMR of Proteins and Nucleic Acids*; John Wiley & Sons: New York, 1986; p 292.
(2) Karplus, M. *J. Chem. Phys.* **1959**, *30*, 11−18.
(3) Prestegard, J. H.; al-Hashimi, H. M.; Tolman, J. R. *Q. Rev. Biophys.* **2000**, *33* (4), 371−424.
(4) Clore, G. M.; Gronenborn, A. *J. Magn. Reson.* **1982**, *48*, 402−417.
(5) Vogel, H. J.; Drakenberg, T.; Forsén, S.; O'Neil, J. D. J.; Hofmann, T. *Biochemistry* **1985**, *24*, 3870−3876.
(6) Kellenbach, E.; Maler, B. A.; Yamamoto, K. R.; Boelens, R.; Kaptein, R. *FEBS* **1991**, *291*, 367−370.
(7) Cass, A. E. G.; Galdes, A.; Hill, H. A. O.; McClelland, C. E.; Storm, C. B. *FEBS Lett.* **1978**, *94*, 311−314.
(8) Blake, P. R.; Lee, B.; Summers, M. F.; Adams, M. W.; Park, J. B.; Zhou, Z. H.; Bax, A. *J. Biomol. NMR* **1992**, *2* (5), 527−533.
(9) Utschig, L.; Bryson, J.; O'Halloran, T. *Science* **1995**, *268*, 380−385.
(10) Coleman, J. E. *Methods Enzymol.* **1993**, *227*, 16−43.
(11) Neuhaus, D.; Wagner, G.; Vasak, M.; Kagi, J. H. R.; Wuthrich, K. *Eur. J. Biochem.* **1984**, *143* (3), 659−667.
(12) Frey, M. H.; Wagner, G.; Vasak, M.; Sorensen, O. W.; Neuhaus, D.; Worgotter, E.; Kagi, J. H. R.; Ernst, R. R.; Wuthrich, K. *J. Am. Chem. Soc.* **1985**, *107* (24), 6847−6851.
(13) Pan, T.; Coleman, J. *PNAS* **1990**, *87* (6), 2077−2081.
(14) Gardner, K. H.; Pan, T.; Narula, S.; Rivera, E.; Coleman, J. E. *Biochemistry* **1991**, *30* (47), 11292−302.
(15) Gardner, K. H.; Coleman, J. E. *J. Biomol. NMR* **1994**, *4* (6), 761−74.
(16) Blake, P. R.; Park, J. B.; Adams, M. W. W.; Summers, M. F. *J. Am. Chem. Soc.* **1992**, *114* (12), 4931−4933.
(17) Live, D.; Armitage, I. M.; Dalgarno, D. C.; Cowburn, D. *J. Am. Chem. Soc.* **1985**, *107*, 1775−1777.
(18) Hess, B.; Haeckel, R. *Nature* **1967**, *214* (90), 848−849.
(19) Nowak, T.; Mildvan, A. S. *Biochemistry* **1972**, *11* (15), 2819−2828.
(20) Shiman, R.; Draper, D. E. *J. Mol. Biol.* **2000**, *302* (1), 79−91.

of heavy metal derivatives.[22,24] While many metal binding sites have been characterized in this way, a spectroscopic technique that eliminates the need for formation of single crystals would expand the experimental arsenal with which monovalent cation sites could be studied.

A solution NMR method for probing monovalent cation sites, using $^{15}NH_4^+$ as a K^+ replacement, has been developed. This technique allows direct observation of bound cations and determination of their possible ligands, independent of whether the $^{15}NH_4^+$ is in fast or slow exchange with the biomacromolecule.[37−39] However, the experiments are most effective at low pH ranges. Therefore, the use of established $^{15}NH_4^+$ NMR methods may prove difficult in many cases. Accordingly, a set of NMR methods is desirable that enables the direct observation of bound monovalent metals, allows localization of their binding site(s), and permits differentiation between monovalent cations at distinct binding sites. Ideally, this technique should also be relatively insensitive to solution conditions, such as pH. A spin-$^1/_2$ nucleus well-suited for developing methods that meet these criteria is thallium ($^{205}Tl^+$), a monovalent metal whose strong anomalous signal and ability to replace K^+ have made it useful in X-ray crystallography and biochemistry.[21,22,40]

Thallium's propensity to substitute for K^+ at its binding sites is due largely to the similar chemical properties of the two metals: atomic radius (1.33 Å for K^+ vs 1.40 Å for Tl^+), dehydration energy (80 kcal/mol vs 82 kcal/mol), bond lengths (2.4−2.7 Å), and ability to support irregular coordination geometries.[41−43] Tl^+ has been shown to bind more tightly than K^+ and to support enzymatic activity, in many cases to the same level as K^+.[44−48] There is a limited precedent for using direct detect ^{205}Tl NMR to study monovalent binding sites in proteins and membrane channels,[40,49−51] but as of yet, only preliminary studies have been performed on nucleic acid systems.[45,52] Identification and characterization of monovalent cation binding sites require an experiment capable of correlating the NMR signal from the monovalent metal with those from the nucleic acid. Despite the noted examples of J-correlations between protons and the divalent surrogates $^{113}Cd^{2+}$ and $^{199}Hg^{2+}$, there have been no reports of scalar couplings between protons and ^{205}Tl in biological systems.

We have used ^{205}Tl NMR to directly examine the monovalent binding sites of the 7.6 kDa G-quadruplex, $d(G_4T_4G_4)_2$, from the telomeric sequence of the ciliate *Oxytricha nova*. G-quadruplex sequences are commonly found in the telomeric DNA of various organisms and in immunoglobulin switch regions.[53,54] G-quadruplexes are characterized by consecutive stacks of four planar, hydrogen-bonded guanine nucleotides, called G-quartets (Figure 1a). G-quadruplexes contain varying numbers of G-quartets and can be formed from between one and four strands of DNA or RNA. The strands are either parallel or antiparallel and contain a variety of loop structures. The G-quadruplex formed by $d(G_4T_4G_4)_2$ is a homodimeric, antiparallel structure with four consecutively stacked G-quartets and diagonal loops at either end (Figure 1b). The formation of this fold results in a rotational symmetry axis that bisects the region between the two inner G-quartet planes (Figure 1c).

When stabilized by the presence of K^+ or NH_4^+ these cations are coordinated between two consecutive G-quartet planes, rather than within the plane of a single G-quartet (Figure 1c). This mode of cation binding was observed in an X-ray structure of the K^+-form of $d(G_4T_4G_4)_2$, reported by Neidle and co-workers.[55] In addition to these three binding sites, a K^+ ion was coordinated by each thymine loop, resulting in five K^+ ions per G-quadruplex.[55] Solution studies of the NH_4^+-form by Feigon and co-workers have provided evidence for three NH_4^+ ions per G-quadruplex (none in the thymine loops) bound in a manner similar to the K^+ coordination.[37,56]

Here, direct detection of ^{205}Tl NMR signals provides evidence that the G-quadruplex $d(G_4T_4G_4)_2$ binds Tl^+ ions and that, similar to the parallel G-quadruplex $d(TG_4T)_4$,[45] this binding can be observed in a ^{205}Tl direct detection experiment. To demonstrate the K^+-like nature of Tl^+ in this biological setting, the solution structure of the G-quadruplex in the presence of Tl^+ has been determined. A $^1H-^{205}Tl$ spin-echo difference experiment has been developed and used to detect the presence of $^1H-^{205}Tl$ scalar couplings. Based on these $^1H-^{205}Tl$ scalar

(21) Basu, S.; Strobel, S. A. *RNA* **1999**, *5* (11), 1399−1407.
(22) Basu, S.; Rambo, R. P.; Strauss-Soukup, J.; Cate, J. H.; Ferre-D'Amare, A. R.; Strobel, S. A.; Doudna, J. A. *Nat. Struct. Biol.* **1998**, *5* (11), 986−992.
(23) Adams, P. L.; Stahley, M. R.; Kosek, A. B.; Wang, J.; Strobel, S. A. *Nature* **2004**, *430* (6995), 45−50.
(24) Conn, G. L.; Gittis, A. G.; Lattman, E. E.; Misra, V. K.; Draper, D. E. *J. Mol. Biol.* **2002**, *318* (4), 963−973.
(25) Mattai, J.; Hauser, H.; Demel, R. A.; Shipley, G. G. *Biochemistry* **1989**, *28* (5), 2322−2330.
(26) Tessier, C.; Quinn, P.; Koumanov, K.; Trugnan, G.; Rainteau, D.; Wolf, C. *Eur. Biophys. J.* **2004**, *33* (6), 513−521.
(27) Toner, M.; Vaio, G.; McLaughlin, A.; McLaughlin, S. *Biochemistry* **1988**, *27* (19), 7435−7443.
(28) Coughlin, R. T.; Tonsager, S.; McGroarty, E. J. *Biochemistry* **1983**, *22* (8), 2002−2007.
(29) Roux, M.; Bloom, M. *Biochemistry* **1990**, *29* (30), 7077−7089.
(30) Moulik, S. P.; Khan, D. P. *Carbohydr. Res.* **1975**, *41*, 93−104.
(31) Kitamura, N.; Ikekita, M.; Sato, T.; Akimoto, Y.; Hatanaka, Y.; Kawakami, H.; Inomata, M.; Furukawa, K. *Proc. Natl. Acad. Sci. U.S.A.* **2005**, *102* (8), 2796−2801.
(32) Kano, K.; Kitae, T.; Shimofuri, Y.; Tanaka, N.; Mineta, Y. *Chemistry* **2000**, *6* (15), 2705−2713.
(33) Lerner, L.; Torchia, D. A. *J. Biol. Chem.* **1986**, *261* (27), 12706−12714.
(34) Nolan, J. M.; Pace, N. R. *Nucleic Acids Mol. Biol.* **1996**, *10*, 109−128.
(35) Pyle, A. M. Catalytic Reaction Mechanisms and Structural Features of Group II Intron Ribozymes. In *Nucleic Acids and Molecular Biology*; Eckstein, F., Lilley, D. M., Eds.; Vol. 10, pp 75−107.
(36) Nissen, P.; Hansen, J.; Ban, N.; Moore, P. B.; Steitz, T. A. *Science* **2000**, *289* (5481), 920−930.
(37) Hud, N. V.; Schultze, P.; Sklenar, V.; Feigon, J. *J. Mol. Biol.* **1999**, *285* (1), 233−243.
(38) Hud, N. V.; Sklenar, V.; Feigon, J. *J. Mol. Biol.* **1999**, *286* (3), 651−660.
(39) Hud, N. V.; Schultze, P.; Feigon, J. *J. Am. Chem. Soc.* **1998**, *120* (25), 6403−6404.
(40) Loria, J. P.; Nowak, T. *Biochemistry* **1998**, *37* (19), 6967−6974.
(41) Pauling, L. The nature of the chemical bond and the structure of molecules and crystals. *An introduction to modern structural chemistry*, 3rd ed.; Cornell University Press: Ithaca, NY, 1960; p 644.
(42) Cox, B. G.; Schneider, H. *Coordination and transport properties of macrocyclic compounds in solution*; Elsevier: Amsterdam, New York, 1992; p 420.
(43) Brown, I. D. *Acta Crystallogr., Sect. B* **1988**, *44*, 545−553.
(44) Douglas, K. T.; Bunni, M. A.; Baindur, S. R. *Int. J. Biochem.* **1990**, *22* (5), 429−438.
(45) Basu, S.; Szewczak, A. A.; Cocco, M.; Strobel, S. A. *J. Am. Chem. Soc.* **2000**, *122* (13), 3240−3241.
(46) Hultin, T.; Naslund, P. H. *Chem. Biol. Interact.* **1974**, *8* (5), 315−328.
(47) Hultin, T.; Naslund, P. H. *Acta Biol. Med. Ger.* **1974**, *33* (5−6), 753−760.
(48) Urry, D. W.; Trapane, T. L.; Venkatachalam, C. M.; Prasad, K. U. *Can. J. of Chem.* **1985**, *63* (7), 1976−1981.
(49) Hinton, J. F.; Young, G.; Millett, F. S. *Biochemistry* **1982**, *21* (4), 651−654.
(50) Hinton, J. F.; Whaley, W. L.; Shungu, D.; Koeppe, R. E., II; Millett, F. S. *Biophys. J.* **1986**, *50* (3), 539−544.
(51) Reuben, J.; Kayne, F. J. *J. Biol. Chem.* **1971**, *246* (20), 6227−6234.
(52) Feigon, J.; Butcher, S. E.; Finger, L. D.; Hud, N. V. *Methods Enzymol.* **2001**, *338*, 400−420.
(53) Williamson, J. R. *Annu. Rev. Biophys. Biomol. Struct.* **1994**, *23*, 703−730.
(54) Sen, D.; Gilbert, W. *Nature* **1988**, *334* (6180), 364−366.
(55) Haider, S.; Parkinson, G. N.; Neidle, S. *J. Mol. Biol.* **2002**, *320* (2), 189−200.
(56) Schultze, P.; Hud, N. V.; Smith, F. W.; Feigon, J. *Nucleic Acids Res.* **1999**, *27* (15), 3018−3028.

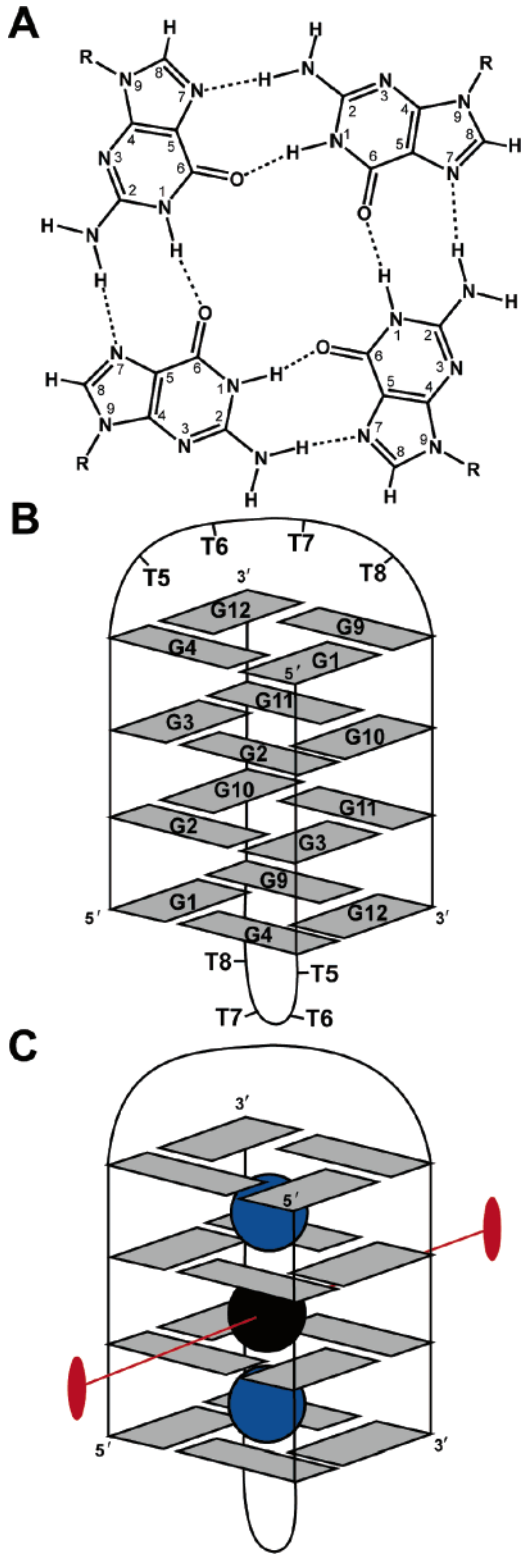

Figure 1. Schematic of G-quartet and the G-quadruplex, $d(G_4T_4G_4)_2$. (A) The structure of a G-quartet formed by four guanine nucleotides. The base atoms have been numbered for convenience. (B) The dimer of $d(G_4T_4G_4)_2$ contains four G-quartets. The diagonal loops are composed of thymine nucleotides. (C) Binding of K^+/NH_4^+ cations (black or blue) to $d(G_4T_4G_4)_2$ is shown.[37,55,56] Only the cations which bind between successive G-quartet planes are pictured. The red line indicates the rotational symmetry plane that bisects the middle cation. The outer cations are colored blue to emphasize their equivalence.

couplings, resonance assignments of the three $^{205}Tl^+$ cations coordinated between G-quartet planes were made.

Methods

Sample Preparation. Chemically synthesized DNA oligonucleotides d(GGGGTTTTGGGG) were purchased (Keck, Yale University) and desalted using Sep-Pak reversed-phase C18 desalting cartridges (Waters, USA). The DNA oligonucleotides were eluted from the C18 columns in 40% (v/v) acetonitrile/water and lyophilized. The DNA was then dissolved to a final concentration of ~500 μM in a solution of 50 mM $TlNO_3$, 100 μM EDTA-d_{12}, and either 10% or 100% D_2O. G-quadruplex formation was facilitated by heating the solutions to 363 K for 15 min followed by slow cooling to 277 K. The solutions were concentrated to about 2.5 mM quadruplex (~5 mM DNA strand) by centrifugation in a Centricon 3 kDa NMWL Centrifugal Filter Unit (Millipore, USA). In some samples, G-quadruplexes were formed in 50 mM NaH_2PO_4 and the Na^+ was exchanged with 50 mM $TlNO_3$ during concentration. G-quadruplexes formed in this manner produced similar ^1H and ^{205}Tl spectra to those formed initially in $TlNO_3$. A K^+ version was also prepared with 50 mM KH_2PO_4 substituted for $Tl-NO_3$. The sample pH was adjusted to 6.5 with H_2PO_4 or CD_3COOD. Monovalent cation titrations using cesium and tetramethylammonium (TMA) were performed by adding small amounts of concentrated solutions of $CsNO_3$ and $TMA-NO_3$ to the G-quadruplex. The total change in DNA concentration due to dilution was not more than 10%. NMR peak areas were corrected for this small amount of sample dilution.

Structure Determination of the G-Quadruplex in Tl^+. NMR experiments were performed on a Varian Unity Plus (14.0 T) spectrometer and a Unity Inova (11.7 T) spectrometer equipped with a cryogenically cooled probe. A $^1H-^1H$ NOESY[57−59] (with mixing times, $\tau_m = 80-350$ ms), DQF−COSY,[57−59] and HOHAHA[57−61] spectra with WATERGATE[57] water suppression and States-TPPI[62,63] frequency discrimination were collected using 2408 $t_2 \times 330$ t_1 points and a spectral width of 8000−9400 Hz in both dimensions. For each t_1 increment, 32−64 scans were acquired. The temperature was regulated at 298 K. Exchangeable protons were assigned from a NOESY collected at 278 K in 10% D_2O. Backbone assignments were aided with a $^{31}P-^1H$ CT-COSY[64] acquired with 2500 $t_2 \times 74$ t_1 points with respective spectral widths of 2500 and 1500 Hz. A total of 264 scans were acquired for each t_1 increment. All experiments were performed on the G-quadruplex formed in the presence of $TlNO_3$.

Distance calibration of NOE peak intensities was performed by semiquantitative methods using cross-peaks corresponding to fixed distances assuming an r^{-6} relationship between peak intensity and distance. After using characteristic NOE cross-peaks described by Feigon and co-workers to verify that the topology of the G-quadruplex is a diagonally looped homodimer, the solution structure of the K^+-form of $d(G_4T_4G_4)_2$ (PDB accession 1K4X) was used to assign cross-peaks residing near the dyad axis.[56,65,66] NOE constraints were duplicated for the symmetrically equivalent pair of protons in the G-quadruplex dimer. ^1H scalar couplings, used as dihedral angle restraints, were calculated from DQF-COSY spectra based on previously described methods.[67]

The solution structure of $d(G_4T_4G_4)_2$ was determined using CNS.[68] These calculations incorporated NOE derived distance constraints, scalar coupling constants, known dihedral angles, hydrogen-bonds, and

(57) Piotto, M.; Saudek, V.; Sklenar, V. *J. Biomol. NMR* **1992**, *2* (6), 661−665.
(58) Brown, S. C.; Weber, P. L.; Mueller, L. *J. Magn. Reson.* **1988**, *77* (1), 166−169.
(59) Altieri, A. S.; Byrd, R. A. *J. Magn. Reson. B* **1995**, *107* (3), 260−266.
(60) Cavanagh, J.; Rance, M. *J. Magn. Reson.* **1992**, *96* (3), 670−678.
(61) Rance, M. *J. Magn. Reson.* **1987**, *74* (3), 557−564.
(62) States, D. J.; Haberkorn, R. A.; Ruben, D. J. *J. Magn. Reson.* **1982**, *48* (2), 286−292.
(63) Marion, D.; Wuthrich, K. *Biochem. Biophys. Res. Commun.* **1983**, *113* (3), 967−974.
(64) Sklenar, V.; Miyashiro, H.; Zon, G.; Miles, H. T.; Bax, A. *FEBS Lett.* **1986**, *208* (1), 94−98.
(65) Smith, F. W.; Feigon, J. *Biochemistry* **1993**, *32* (33), 8682−8692.
(66) Smith, F. W.; Feigon, J. *Nature* **1992**, *356* (6365), 164−168.
(67) Kim, Y. M.; Prestegard, J. H. *J. Magn. Reson.* **1989**, *84* (1), 9−13.

noncrystallographic symmetry constraints. Initial structures were generated using distance geometry with simulated annealing. The structure refinement proceeded by rounds of ab initio simulated annealing involving high-temperature torsion dynamics (2000 K for 60 ps with 15 fs time steps) followed by a Cartesian cooling stage (1000 K for 5 ps with 5 fs time steps) and restrained molecular dynamics (10 cycles of 200 steps each).

^{205}Tl NMR Spectroscopy. All ^{205}Tl NMR experiments performed at 11.7 T (288 MHz ^{205}Tl) used a Varian Inova wide bore spectrometer. Direct detection ^{205}Tl NMR experiments were performed with a Nalorac direct detection dual broadband probe using a pulse-acquire experiment with 100 000 acquisitions, a 60 kHz spectral width, and a 500 ms recycle delay. All ^{205}Tl spectra were externally referenced to samples containing 50 mM $TlNO_3$, 100 μM EDTA, 10% D_2O, and identical concentrations of buffers and salts used in the actual experiment. The ^{205}Tl NMR spectrum collected at 7.0 T (173 MHz ^{205}Tl) using a Varian Unity spectrometer was performed in the Department of Chemistry and Biochemistry at the University of Notre Dame in a similar manner.

The exchange rate of $^{205}Tl^+$ coordinated by the G-quadruplex with the bulk solution was determined using magnetization transfer experiments.[69−71] The free ^{205}Tl resonance was saturated with a low power selective pulse for variable times (0, 50, 100, 200, 300, 400, and 500 ms). The effect of this saturation pulse on the bound ^{205}Tl resonances was measured with a $\pi/2$ pulse immediately following the saturation period. For each saturation time, a reference spectrum was acquired in which the frequency of the saturating pulse was placed upfield of the free ^{205}Tl resonance. A total of 25 000 interleaved acquisitions were collected for each saturation time with a 1 s recycle delay. The magnetization transfer data were analyzed using nonlinear least-squares regression, which was performed in MATLAB (Mathworks, Inc.) using the Levenberg−Marquardt[72−74] method.

^{1}H−^{205}Tl Scalar Coupling. The ^{1}H−^{205}Tl spin-echo difference experiments were performed using a Nalorac indirect detection broadband probe with a home-built inductor stick for tuning the broadband channel to the ^{205}Tl frequency (288 MHz/11.7T). A second high-frequency amplifier was employed to achieve the ^{205}Tl frequency and allow simultaneous RF pulsing on ^{1}H and ^{205}Tl nuclei. The spin-echo difference experiments were acquired in an interleaved manner as described in the caption to Figure 6. Typically, 30 000−50 000 acquisitions were performed although a signal can be observed above the background noise in as few as 10 000 acquisitions. The delay for *J*-coupling evolution was set to 15, 40, and 100 ms.

All NMR data were processed in NMRPipe,[75] and resonance assignments were performed using Sparky.[76] NMR line shapes and peak intensities were analyzed using NMRPipe and an in-house written MATLAB code.

Results

Solution Structure of the Tl^+ Form of $d(G_4T_4G_4)_2$. The solution structure of $d(G_4T_4G_4)_2$ was determined to assess the ability of Tl^+ to support formation of native, K^+-like G-quadruplexes. The total number of nonredundant NOE distance restraints per DNA strand was 395. Of these, 192 occurred between different bases, 38 were long range (greater than one base apart), and 56 involved exchangeable protons (Table 1). Refinement of the Tl^+-form of $d(G_4T_4G_4)_2$ in CNS proceeded by ab initio simulated annealing using NOE derived distance constraints. The final 10 lowest energy conformers had no distance violations > 0.5 Å and no dihedral angle violations > 5° (Table 1) and were deposited in the PDB under accession number 2AKG. The RMSD of these 10 structures was 0.76 ± 0.16 Å for all atoms (Figure 2). In addition, the RMSD of the mean Tl^+ structure with the mean K^+ structure is 1.17 ± 0.13 Å. Chemical shift patterns in the H1 (imino), H8/H6 (aromatic), and H1′ regions of the Tl^+-form are very similar to those reported for the K^+ NMR structure,[56] with the aromatic-H1′ pattern of connectivities being nearly identical (data not shown).

The Tl^+-form of $d(G_4T_4G_4)_2$ is an antiparallel G-quadruplex with diagonally looped thymines at either end (Figure 2). The guanine nucleotides are in alternating *syn*−*anti* conformations, and the G-quadruplex has one narrow groove (11.7 Å wide, from C5′ to C5′), two intermediate grooves (14.1 Å), and a single, wide groove (17.3 Å). All T nucleotides are in *anti*

Table 1. Experimental Structure Ensemble Statistics for the Tl^+-Form of $d(G_4T_4G_4)_2$

NOE restraints	
total	395
intraresidue	241
interresidue	154
long-range	38
exchangeable	56
average violations/structure	
NOE (>0.5 Å)	0 ± 0
dihedrals (>5°)	0 ± 0
ensemble RMSD (Å)	
all atoms	0.76 ± 0.16

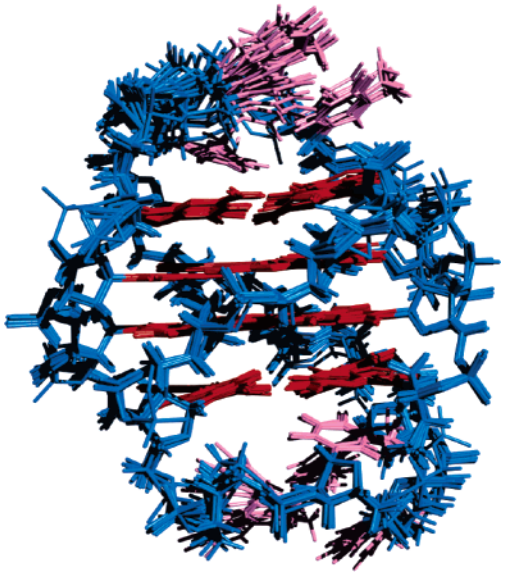

Figure 2. Solution NMR structure of the Tl^+-form of $d(G_4T_4G_4)_2$ (PDB 2AKG). The 10 lowest energy conformers are shown with the guanine nucleotides in red, thymine nucleotides in purple, and the deoxyribose-phosphate backbone in blue. The figure was prepared with Pymol (DeLano Scientific, 2002) and POV-Ray (Persistence of Vision Raytracer Pty. Ltd., 1994).

(68) Brunger, A. T.; Adams, P. D.; Clore, G. M.; DeLano, W. L.; Gros, P.; Grosse-Kunstleve, R. W.; Jiang, J. S.; Kuszewski, J.; Nilges, M.; Pannu, N. S.; Read, R. J.; Rice, L. M.; Simonson, T.; Warren, G. L. *Acta Crystallogr., Sect. D* **1998**, *54* (Pt 5), 905−921.
(69) Forsen, S.; Hoffman, R. A. *J. Chem. Phys.* **1964**, *40* (5), 1189−1196.
(70) Forsen, S.; Hoffman, R. A. *J. Chem. Phys.* **1963**, *39* (11), 2892−2901.
(71) Campbell, I. D.; Dobson, C. M.; Ratcliffe, R. G. *J. Magn. Reson.* **1977**, *27* (3), 455−463.
(72) Levenberg, K. *Quart. Appl. Math.* **1944**, *2*, 164−168.
(73) Marquardt, D. W. *J. Soc. Ind. Appl. Math.* **1963**, *11* (2), 431−441.
(74) Gill, P. E.; Murray, W.; Wright, M. H. *Practical optimization*; Academic Press: London, New York, 1981; pp xvi, 401.
(75) Delaglio, F.; Grzesiak, S.; Vuister, G.; Zhu, G.; Pfeifer, J.; Bax, A. *J. Biomol. NMR* **1995**, *6*, 277−293.
(76) Goddard, T.; Kneller, D. G. *SPARKY 3*; University of California, San Francisco.

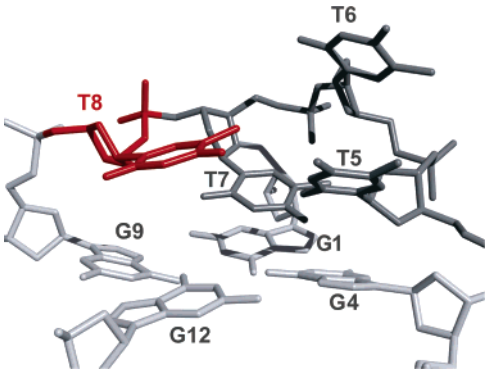

Figure 3. Thymine loops of the Tl^+-form of $d(G_4T_4G_4)_2$. T8 (red) stacks above G12 of the nearby G-quartet. G4 and G9 are from the same DNA strand as T8, whereas G1 and G12 are from the opposing DNA strand. The figure was prepared with Pymol (DeLano Scientific, 2002) and POV-Ray (Persistence of Vision Raytracer Pty. Ltd., 1994).

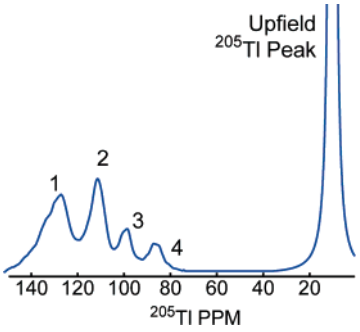

Figure 4. ^{205}Tl NMR spectrum of the Tl^+-form of $d(G_4T_4G_4)_2$. The sample contained 50 mM $Tl-NO_3$ at pH 6.5 and was regulated at 298 K. The experiment was acquired at 11.7 T with 100,000 scans and a spectral width of 60 kHz. The downfield peaks are numbered 1−4.

conformations, and the H1′−H2′, H2″ scalar couplings indicate all deoxyribose sugars exist predominately in the C2′-endo conformation.

In the presence of Tl^+, T8 in the loop region stacks just above and parallel to the plane of the nearby G-quartet, composed of G4 and G9 from the identical strand and G1 and G12 from the opposing DNA strand (Figure 3). NOE cross-peaks (not shown) between the T8 methyl group and the imino (H1) protons of G1, G4, G9, and G12 define the loop conformation. The thymine loop regions of the K^+ and Tl^+ structures share a high degree of similarity with T8 stacking above G12 of the proximal G-quartet (Figure 3) in both structures. The loop region of the Tl^+-form of $d(G_4T_4G_4)_2$ also resembles the reported NMR structure of the NH_4^+-form.[56] In an NMR structure of the Na^+-form of $d(G_4T_4G_4)_2$, T8 is pointed outward in a more extended conformation.[56]

^{205}Tl NMR of $d(G_4T_4G_4)_2$. The NMR observation of $^{205}Tl^+$ ions bound to G-quadruplexes was achieved by direct detection using a pulse-acquire sequence. The one-dimensional ^{205}Tl spectrum of $d(G_4T_4G_4)_2$ shows an intense peak at ~10 ppm and a cluster of four (numbered 1−4) broader peaks centered at about 115 ppm (Figure 4). The line widths (full width at half-height) of these four peaks are 2.7, 1.9, 1.5, and 1.5 kHz for resonances 1−4, respectively. Each of these downfield peaks is resistant to increases in temperature. At 333 K, the intensity of peak 4 decreases slightly, while the heights of peaks 1−3 remain relatively constant up to this temperature (not shown). However, at 338 K, the reported unfolding temperature of the

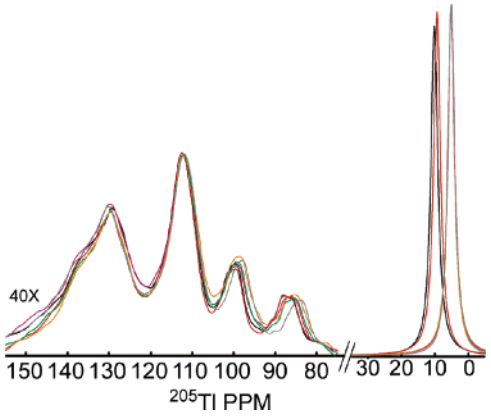

Figure 5. Cs^+ titrations of Tl^+-form of $d(G_4T_4G_4)_2$. Titration of Cs^+ into $d(G_4T_4G_4)_2$ containing 50 mM $Tl-NO_3$ at 298 K. The upfield peak narrows and shifts toward 5 ppm as the concentration of Cs^+ increases. Cs^+ concentrations, relative to Tl^+, are 0:1 (black), 0.5:1 (red), 1:1 (purple), 1.5:1 (green), 2:1 (orange), 6:1 (gray). The downfield resonances are vertically expanded 40-fold relative to the upfield peak.

NH_4^+- and Na^+-forms of the G-quadruplex,[37,77] all four peaks disappear. The position and intensity of these downfield peaks are also resistant to the presence of excess Cs^+ (Figure 5) or tetramethylammonium ion (not shown). In contrast, the upfield Tl^+ resonance is shifted further upfield from 10 to 5 ppm when Cs^+ is added. In addition the line width of the ^{205}Tl resonance narrows from 413 to 386 Hz upon addition of Cs^+. The addition of TMA^+ to the G-quadruplex has similar effects on the upfield ^{205}Tl peak.

The lifetime of $^{205}Tl^+$ at each of the binding sites defined by the four downfield ^{205}Tl resonances was determined as described by Forsén and Hoffman,[69,70] except that nonlinear least-squares regression was used for parameter fitting. Briefly, the decay of the downfield ^{205}Tl resonances (site A) upon saturation of the bulk ^{205}Tl resonance (site B) for time (t) is given by

$$M_z^A = M_0^A\left[\frac{\tau_{1A}}{\tau_A}e^{(-t/\tau_{1A})} + \frac{\tau_{1A}}{T_{1A}}\right] \quad (1)$$

where M_0^A is the initial magnetization at site A when $t = 0$ and M_z^A is the magnetization as $t \rightarrow \infty$. T_{1A} is the spin-lattice relaxation time at site A, and τ_A is the bound lifetime at site A. T_{1A} and τ_A are related by the equation

$$\frac{1}{\tau_{1A}} = \frac{1}{\tau_A} + \frac{1}{T_{1A}} \quad (2)$$

Combining eqs 1 and 2 yields

$$\frac{M_z^A}{M_0^A} = \left[\left(1 - \frac{\tau_{1A}}{T_{1A}}\right)e^{(-t/\tau_{1A})} + \frac{\tau_{1A}}{T_{1A}}\right] \quad (3)$$

The values of τ_{1A}/T_{1A} and τ_{1A} were determined by nonlinear least-squares regression with eq 3. The results are shown for each of the downfield ^{205}Tl peaks as a function of saturation time of the free ^{205}Tl resonance (Figure 6 and Table 2). From these values, the spin-lattice relaxation time (T_{1A}) and the bound lifetime (τ_A) were determined for the $^{205}Tl^+$ ion bound to each respective site on the G-quadruplex (Table 2). The bound

(77) Deng, H.; Braunlin, W. H. *J. Mol. Biol.* **1996**, *255* (3), 476−483.

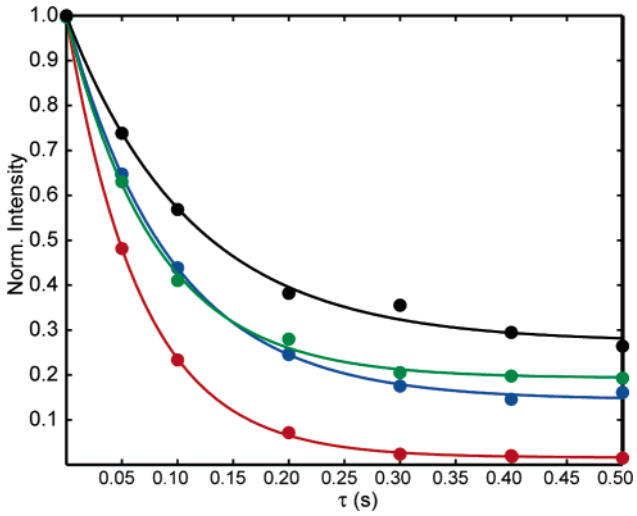

Figure 6. Magnetization transfer experiment. The decay of the intensity of the downfield ^{205}Tl peaks upon saturation of the free ^{205}Tl resonance, for time (τ, seconds). Peaks 1−4 are colored red, blue, green, and black, respectively. Solid lines indicate results of nonlinear least-squares fitting to eq 3 with R^2 = 0.9999, 0.9995, 0.9987, and 0.9965 for peaks 1−4, respectively.

Table 2. Exchange Constants for Bound $^{205}Tl^+$ Ions

	peak 1	peak 2	peak 3	peak 4
τ_{1A}/T_{1A}	0.16 ± 0.01	0.14 ± 0.02	0.20 ± 0.03	0.27 ± 0.05
τ_{1A}(s)	0.07 ± 0.01	0.09 ± 0.01	0.08 ± 0.01	0.11 ± 0.03
T_{1A}(s)	0.41 ± 0.02	0.64 ± 0.10	0.41 ± 0.09	0.42 ± 0.14
τ_A(s)	0.08 ± 0.01	0.11 ± 0.01	0.10 ± 0.02	0.15 ± 0.06

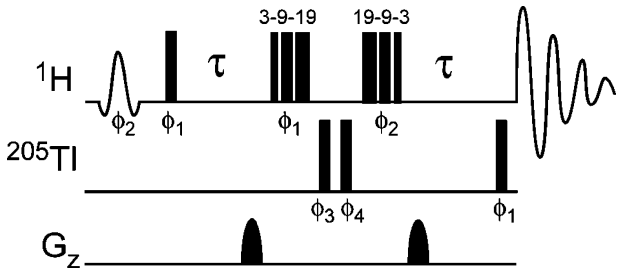

Figure 7. ^{1}H−^{205}Tl spin-echo difference pulse sequence. The sequence is performed in two interleaved parts. In the first half (S_0), $\varphi_1 = \{x,y,-x,-y\}$, $\varphi_2 = \{-x,-y,x,y\}$, $\varphi_3 = \{x\}$, $\varphi_4 = \{-x\}$, and $\varphi_{rec} = \{x,y,-x,-y\}$. For the S_1 experiment, $\varphi_4 = \{x\}$. All pulses were additionally phase-cycled using the CYCLOPS scheme.[79] The experiment was performed with τ = 15, 40, and 100 ms.

lifetimes range from 80 ± 10 ms for peak 1 to 155 ± 65 ms for peak 4. The errors in the fits are based on a 95% confidence interval.

To further investigate the nature of the downfield ^{205}Tl peaks, we implemented a heteronuclear ^{1}H−^{205}Tl spin-echo difference experiment (Figure 7) to look for potential H−Tl interactions.[8,16] To maintain water suppression while maximizing signal from solvent-exchangeable protons, a water-selective sinc pulse and gradient-tailored 3−9−19 pulse train[78] were incorporated into the pulse sequence. The experiment was performed in a two-part, interleaved fashion with either complete recoupling of heteronuclear J modulation when $\phi_4 = -x$, resulting in a ^{1}H signal intensity corresponding to

$$S_0 = e^{(-2\tau/T_2)} \quad (4)$$

or with the occurrence of heteronuclear J modulation when $\phi_4 = x$, resulting in the ^{1}H signal intensity

$$S_1 = e^{(-2\tau/T_2)}\cos(2\pi J_{H-Tl}\tau) \quad (5)$$

where T_2 is the proton transverse relaxation time. The scalar coupling constant, J_{H-Tl}, is determined from

$$\frac{S_0 - S_1}{S_0} = 1 - \cos(2\pi J_{H-Tl}\tau) = 2\sin^2(\pi J_{H-Tl}\tau) \quad (6)$$

This spin-echo difference experiment was performed using bandwidth selective square ^{205}Tl pulses (5.7 kHz, 3 kHz, 2.5 kHz, and 3 kHz) for each of the downfield ^{205}Tl peaks, 1−4, respectively. Variations in the identity and magnitude of the scalar couplings are observed between $^{205}Tl^+$ peaks 2 and 3 and aromatic and imino protons of the G-quadruplex (Figure 8a−c). For peak 2, scalar couplings are observed to all G aromatic protons except G4 and G12 and to the imino protons for G1/G9 (assignment ambiguous), G2, and G4 (Figure 8b, c and Table 3). ^{1}H−^{205}Tl scalar couplings for peak 3 are observed to the G2, G3, G10, and G11 aromatic H8 protons and to the G2 and G10 imino protons (Figure 8b, c and Table 3). These couplings are small and range from 0.34 to 0.95 Hz (Table 2). No signal is observed in the $S_0 - S_1$ spectrum when K^+ is used in place of Tl^+, consistent with these couplings arising from a ^{1}H−^{205}Tl mediated effect (Figure 8a). No couplings between ^{1}H and ^{205}Tl were observed for ^{205}Tl peaks 1 and 4 (Figure 8b, c).

Discussion

Comparison to Other d(G$_4$T$_4$G$_4$)$_2$ Structures. The Tl^+-form of d(G$_4$T$_4$G$_4$)$_2$ closely resembles the NMR structure of the K^+-form,[56] with an overall RMSD between the two of 1.17 ± 0.13 Å. Thus, Tl^+ can effectively mimic the action of K^+ in promoting formation of nativelike G-quadruplexes. The solution structures of the Tl^+-, K^+-, and NH_4^+-forms of d(G$_4$T$_4$G$_4$)$_2$ differ from the Na^+-form of the G-quadruplex. These variations have been attributed to the smaller ionic radius of Na^+, which alters the way this cation binds within the G-quadruplex.[56] The structural similarities between the Tl^+- and K^+-forms of d(G$_4$T$_4$G$_4$)$_2$ are consistent with their similar physical and chemical properties.

Assignment of ^{205}Tl Peaks Based on ^{1}H−^{205}Tl Scalar Couplings. The observation that small ^{1}H−^{205}Tl couplings exist presents possibilities to localize monovalent cation binding sites in macromolecules and to investigate how specific monovalent sites respond to solution perturbations, mutation, or ligand binding. In the experiments described here, ^{205}Tl selective pulses were incorporated into the ^{1}H−^{205}Tl spin-echo difference experiment so that the ^{205}Tl peaks could be assigned to monovalent binding sites within the G-quadruplex. By mapping the results of these experiments onto the structure of d(G$_4$T$_4$G$_4$)$_2$, the identities of two of the four ^{205}Tl peaks can be determined. For peak 3, ^{1}H−^{205}Tl scalar couplings are only observed to the aromatic and imino protons of the inner two G-quartet planes (Figure 8b, c), so this peak can be assigned to the innermost G-quadruplex binding site (Figure 9a). For the ^{205}Tl resonance corresponding to peak 2, couplings are observed to guanine aromatic and imino protons throughout all four G-quartet planes

(78) Sklenar, V.; Piotto, M.; Leppik, R.; Saudek, V. *J. Magn. Reson. A* **1993**, *102* (2), 241−245.

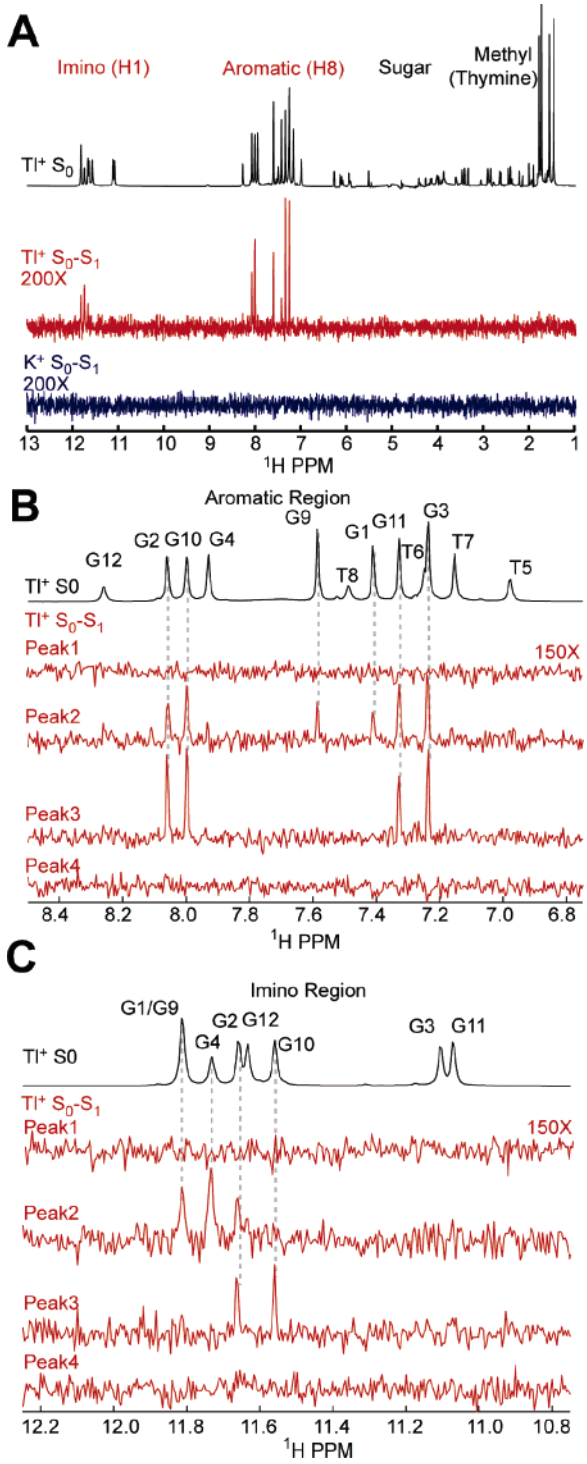

Figure 8. $^{1}H-^{205}Tl$ scalar couplings. (A) The reference, S_0, and difference, $S_0 - S_1$, spectra for the Tl^+-form of $d(G_4T_4G_4)_2$ (black and red). The negative control, $S_0 - S_1$ spectrum of the K^+-form of $d(G_4T_4G_4)_2$ is shown in blue. (B) An expanded region showing the ^{205}Tl scalar couplings to the aromatic protons for each of the downfield ^{205}Tl peaks (1−4) (red) is below the reference spectrum shown in black. (C) An expanded region showing the ^{205}Tl scalar couplings to the imino protons for each of the downfield ^{205}Tl peaks (1−4) using the same color scheme as that in (B). All difference spectra, $S_0 - S_1$, are vertically expanded 200× (A) and 150× (B and C).

(Figure 8b, c). Assuming this peak represents a single ^{205}Tl binding site, the only assignment consistent with the observed couplings are the two symmetrically related outer binding sites (Figure 9b). The assignment of peaks 2 and 3 to the respective

Table 3. Magnitude of $^{1}H-^{205}Tl$ Scalar Couplings (Hz) to Individual ^{205}Tl Peaks

	guanine residue	peak 2	peak 3
imino	G1/9	0.46 ± 0.04	
	G2	0.54 ± 0.04	0.51 ± 0.06
	G4	0.95 ± 0.06	
	G10		0.44 ± 0.03
aromatic	G1	0.34 ± 0.06	
	G2	0.44 ± 0.05	0.52 ± 0.03
	G3	0.49 ± 0.02	0.65 ± 0.01
	G9	0.34 ± 0.04	
	G10	0.49 ± 0.04	0.56 ± 0.02
	G11	0.47 ± 0.03	0.40 ± 0.02

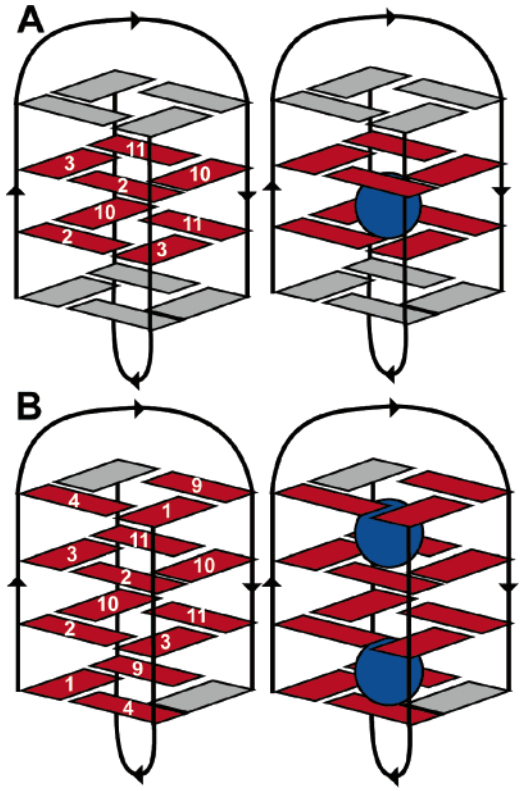

Figure 9. Location of $^{1}H-^{205}Tl$ scalar couplings for ^{205}Tl peaks 2 and 3. (A) On the left, the couplings from ^{205}Tl peak 3 are observed to imino and aromatic protons on bases (red) located within the middle two G-quartet planes. The assignment of peak 3 to a specific monovalent cation (blue) is shown on the right. (B) The *J*-couplings between ^{205}Tl peak 2 and imino or aromatic protons are located on bases found in all four G-quartet planes. The proposed assignment of peak 2 (blue sphere) is shown on the right.

outer and inner G-quadruplex cation sites is also consistent with the relative areas (2:1) of these peaks in the direct detection ^{205}Tl spectrum (Figure 4). Peaks 1 and 4 do not have any observed couplings to protons in this G-quadruplex and thus cannot be assigned in this fashion (Figure 8b, c). The couplings observed to ^{205}Tl peaks 2 and 3 comprise the first $^{1}H-^{205}Tl$ scalar couplings reported in a biological system.[80]

The detection of small, unresolvable scalar couplings, such as those reported here for proton−metal interactions, requires the sensitivity of a difference experiment. The $^{1}H-^{205}Tl$ scalar couplings between guanine aromatic/imino protons and bound

(79) Hoult, D. I.; Richards, R. E. *Proc. R. Soc. London, Ser. A* **1975**, *344* (1638), 311−340.
(80) Ghosh, P.; Desrosiers, P. J.; Parkin, G. *J. Am. Chem. Soc.* **1998**, *120*, 10416−10422.

$^{205}Tl^+$ cations are all less than 1 Hz (Table 3), with the coupling to the G4 imino proton being the largest, 0.95 ± 0.06 Hz. The spin-echo difference experiment was performed with three different refocusing delays, 15, 40, and 100 ms. The estimation of J_{H-Tl} from these individual experiments is consistent with a cosine modulated coupling interaction (eq 6). The magnitude of these couplings is similar to those detected between either ^{113}Cd or ^{199}Hg and protons in rubredoxin.[8] Some of the expected couplings to imino protons from G3 and G11 and aromatic protons from G4 and G12 are absent. These "missing" imino couplings to either ^{205}Tl peak (Figure 8c) could be caused by a combination of reduced signal-to-noise of these proton resonances and very small scalar coupling values. The absence of aromatic scalar couplings involving G4 and G12 to ^{205}Tl resonance 2 (Figure 8b) is likely due to increased conformational exchange at these sites. Increased motion is particularly noticeable at G12, where conformational exchange results in a reduced number of NOE cross-peaks to this nucleotide (data not shown).

These results indicate that $^{205}Tl^+$ is scalar coupled to both imino (H1) and aromatic (H8) protons, but they do not report on the pathway by which these two interactions occur. Besides covalent bonds, scalar couplings are known to follow hydrogen-bond, coordination, and through-space mediated pathways.[8,16] A discussion of the possible pathways giving rise to these $^1H-^{205}Tl$ scalar couplings requires consideration of the availability of functional groups which could interact with Tl^+, the intricate hydrogen-bonding network of the G-quartets, and the most direct pathway available for these interactions.

We have considered three explanations for the observed guanine imino (H1) couplings. The first involves a direct interaction between the coordinated $^{205}Tl^+$ cations and the imino protons (Figure 10a, blue). Based on the K^+ X-ray structure of $d(G_4T_4G_4)_2$, the distance from the center of the metal cation to the H1 proton is about 3.5 Å.[55] The couplings could also be mediated through the O6 carbonyl group, which coordinates the monovalent cation. This coordination would provide a mechanism for a four-bond coupling (O6−C6, C6−N1, N1−H1) to the imino proton on the same guanine nucleotide (Figure 10a, red). An alternate pathway, beginning with O6 and traversing the O6−H1 hydrogen bond, would result in couplings to an imino proton on a nearby G nucleotide (Figure 10a, green). Of the last two possibilities, the former involves three covalent bonds; the later pathway is shorter but includes a hydrogen bond. There are precedents for scalar couplings similar to both instances.[81,82]

The observation of ^{205}Tl scalar couplings to guanine H8 is unexpected given the distance and/or number of bonds that must be traversed. A direct interaction between ^{205}Tl and the H8 proton seems unlikely because the distance from the monovalent ion-binding site to this proton is 7.7 Å (Figure 10b, blue pathway); the long distance over which couplings are observed also suggests these effects are due to electron orbital couplings and not a dipolar interaction. If the scalar coupling was mediated by the O6 carbonyl ligand, it is six covalent bonds (O6−C6, C6−C5, C5−N7, N7−C8, C8−H8) to the aromatic proton (Figure 10b, red). A total distance of six bonds (five covalent + one coordination) is also quite long, although scalar couplings

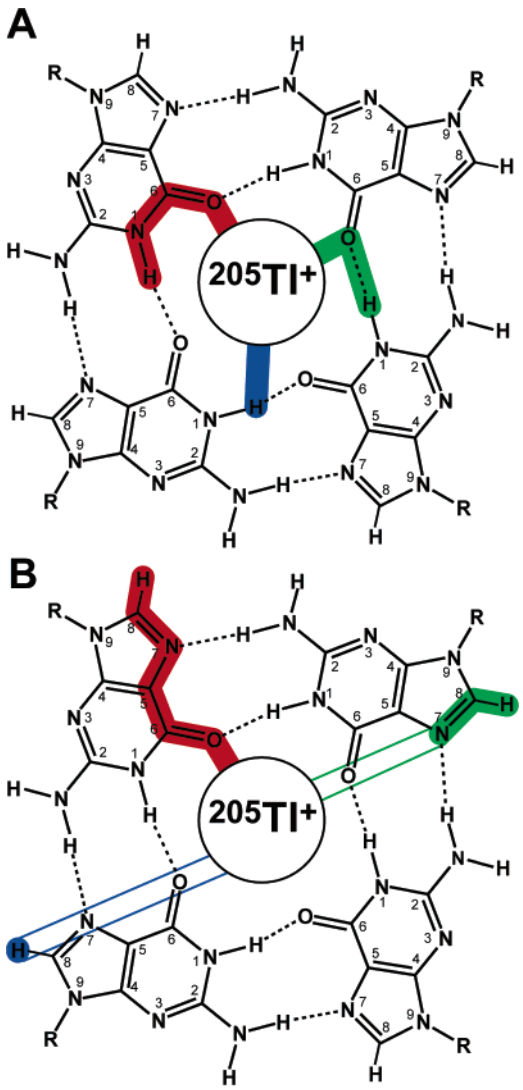

Figure 10. Possible $^1H-^{205}Tl$ scalar coupling mechanisms. (A) Possible mechanisms for imino protons involving direct (blue) and through bond (red and green) pathways. (B) Alternative mechanisms for scalar couplings between ^{205}Tl and aromatic protons are shown in blue, red, and green. Unfilled regions indicate atoms, which are not included in the pathway. Additional details are provided in the text.

have been observed through four[81,83] and five bonds.[8] Another possibility considered here involves interaction of the $^{205}Tl^+$ with the N7 atom and continuation through two bonds (N7−C8, C8−H8) to the aromatic proton (Figure 10b, green). The distance from each of the three $^{205}Tl^+$ cations to the N7 atoms of scalar coupled G bases is about 5.2 Å. This pathway is plausible as the interaction of thallium with guanine N7 has been shown to be favorable.[24,84] Finally, a combination of multiple pathways leading to an averaged, observed coupling cannot be ruled out.

The potential for residual dipolar couplings (RDC) contributing to the observed *J*-coupling, due to the natural magnetic field alignment of the G-quadruplex, was addressed in two ways. First, the magnetic susceptibility, $\Delta\chi$, of the quadruplex was either estimated using the method of Bothner-By[85] and that of

(81) Grzesiek, S.; Cordier, F.; Dingley, A. J. *Methods Enzymol.* **2001**, *338*, 111−33.
(82) Dingley, A. J.; Masse, J. E.; Feigon, J.; Grzesiek, S. *J. Biomol. NMR* **2000**, *16* (4), 279−289.
(83) Liu, A.; Majumdar, A.; Hu, W.; Kettani, A.; Skripkin, E.; Patel, D. *J. Am. Chem. Soc.* **2000**, *122* (13), 3206−3210.
(84) Lee, A. G. *The chemistry of thallium*; Elsevier Pub. Co.: Amsterdam, New York, 1971; p 336.

Bax[86] or was calculated using quantum mechanical methods. Each method gave similar values for $\Delta\chi$. Second, we measured the $^1D_{CH}$ value for the aromatic proton of guanine[87] and estimated the D_{HTl} value using the appropriate scaling factors. For the aromatic proton, H8, which is 7.7 Å from ^{205}Tl, both estimations indicate the contribution of the RDC to the *J*-coupling value ranges from negligible to ~1−2%. For the H1 imino proton (3.5 Å from ^{205}Tl), the RDC contribution could range from ~1% to ~20%. Therefore, for the aromatic proton the *J*-values are essentially free from any residual dipolar contribution, whereas the RDC contribution to the observed imino *J*-coupling is small. However, at higher field or in more strongly aligning media, ^{1}H−^{205}Tl dipolar couplings could be significant and a source of potentially useful information.

Two bound thallium peaks (1 and 4) remain unassigned. The observation of four downfield peaks in the ^{205}Tl direct detection experiment was not expected. Based on solution studies of the NH_4^+ form of $d(G_4T_4G_4)_2$,[37,56] it was anticipated that three ^{205}-Tl^+ cations would bind $d(G_4T_4G_4)_2$, each sandwiched between two adjacent G-quartet planes. Because the outer two binding sites are related by a single rotational symmetry plane (Figure 1c), the anticipated scenario would result in the observation of two downfield ^{205}Tl peaks with relative areas of 2:1 (outer/inner). We have considered three possible explanations for the assignment of ^{205}Tl peaks 1 and 4: (1) the occurrence of ^{205}-Tl−^{205}Tl scalar couplings leading to peak splittings; (2) the existence of high-affinity, $^{205}Tl^+$-specific binding sites within the G-quadruplex grooves; and (3) binding of $^{205}Tl^+$ within the thymine loops.

Homonuclear ^{205}Tl scalar couplings have been observed in the kHz range.[88] Given that binding of metals to the G-quadruplex results in the close juxtaposition of at least three $^{205}Tl^+$ cations, we considered the possibility that ^{205}Tl−^{205}Tl scalar couplings can explain the pattern of the downfield ^{205}Tl peaks. The areas of the downfield peaks do not correspond to any canonical pattern of ^{205}Tl−^{205}Tl peak splittings, even when multiple couplings and peak overlap are considered. To be sure, we also examined the magnetic field dependence of the downfield ^{205}Tl peaks by repeating the direct detection experiment at 7.0 T, 173 MHz ^{205}Tl. The chemical shifts (in ppm) of all ^{205}Tl peaks do not change at this lower magnetic field, ruling out the possibility of ^{205}Tl−^{205}Tl scalar couplings.

It is possible that one or both of the unassigned downfield peaks results from $^{205}Tl^+$ binding to one or more site(s) within the four G-quadruplex grooves. There is a precedent for monovalent cation-specific association in the major and minor grooves of B-form DNA.[38,89,90] One such example involved preferential binding of Tl^+ to the major and minor grooves of G-tract regions.[89] Interestingly, no K^+ cations were assigned to G-quadruplex grooves within the crystal structure of the K^+-form of $d(G_4T_4G_4)_2$.[55] Furthermore, when included in a predominately Na^+-containing crystallization solution, Tl^+ was not reported to bind within the grooves of the parallel-stranded G-quadruplex, $d(TG_4T)_4$, despite its ability to compete effectively for binding sites between the G-quartet planes.[91] It also seems unlikely that nonspecific associations, such as those that would be expected from groove binding, would remain at temperatures as high as 333 K (vide supra). This conclusion is further supported by the invariability of peaks 1−4 to concentrations of Cs^+ or tetramethylammonium ion, which are added to 6- and 4-fold excess of the Tl^+ concentration, respectively. Cs^+ in particular has been shown to have a much higher affinity than K^+ for binding to the G-quadruplex grooves;[92] thus Cs^+ would be expected to displace $^{205}Tl^+$ from any backbone sites and result in a decrease in intensity for that bound ^{205}Tl peak. This effect is not observed. Therefore if Tl^+ binds in the G-quadruplex grooves, it does so with very high affinity and in a manner that has thus far precluded its detection by NMR and X-ray crystallography.

The third possibility, Tl^+ binding within the thymine loops, would be consistent with the aforementioned crystallographic structure of the K^+-form of $d(G_4T_4G_4)_2$.[55] It is important to note that the thymine loops in the K^+ crystal structure are in a slightly different conformation than that in the NMR structures of the K^+- and NH_4^+-forms (and the Tl^+-form reported here) of $d(G_4T_4G_4)_2$.[56] No ^{1}H−^{205}Tl scalar couplings were observed to any thymine protons (Figure 8a−c); however, the absence of ^{1}H−^{205}Tl scalar couplings does not disprove loop binding. The thymine aromatic (H6) protons have elevated transverse relaxation rates compared to the aromatic protons. Thus the lower signal-to-noise associated with faster relaxing nuclei may mask any apparent ^{205}Tl−H6 proton coupling. In addition, there may simply not be a significant amount of orbital interaction between ^{205}Tl and the thymine protons to observe these small couplings. Furthermore, the line shape of ^{205}Tl peak 1 appears non-Lorentzian possibly indicating the presence of inhomogeneous line broadening. Such an effect would further diminish the chances of detecting couplings to nearby protons.

Saturation transfer experiments indicate that peak 4 exchanges slightly faster with free thallium than peaks 1−3. The decreased residence time of peak 4 could contribute to the absence of any observable couplings to this resonance. The measured lifetimes are also likely affected by the exchange of $^{205}Tl^+$ between G-quadruplex sites; however it is difficult to account for this unless the precise exchange pathway is known. Thus, these results provide a good approximation of the bound lifetime of $^{205}Tl^+$ within the G-quadruplex binding sites corresponding to each of the four downfield ^{205}Tl resonances. Based on these NMR experiments we suggest the likely locations of peaks 1 and 4 are in the thymine loops and possibly along one of the quadruplex grooves with at least one of these positions experiencing additional effects of conformational heterogeneity.

Conclusions

We have used heteronuclear ^{1}H−^{205}Tl NMR and direct detection ^{205}Tl NMR to characterize the binding of Tl^+ to $d(G_4T_4G_4)_2$ in a site-specific manner. The results from these studies demonstrate the isomorphous nature of Tl^+ and K^+ and, to our knowledge, constitute the first heteronuclear ^{205}Tl NMR

(85) Lisicki, M. A.; Mishra, P. K.; Bothner-By, A. A.; Lindsey, J. S. *J. Phys. Chem.* **1988**, *92*, 3400−3403.
(86) Bryce, D. L.; Boisbouvier, J.; Bax, A. *J. Am. Chem. Soc.* **2004**, *126*, 10820−10821.
(87) Kung, H. C.; Wang, K. Y.; Goljer, I.; Bolton, P. H. *J. Magn. Reson. B* **1995**, *109*, 323−325.
(88) Hinton, J. F. *Magn. Reson. Chem.* **1987**, *25* (8), 659−669.
(89) Howerton, S. B.; Sines, C. C.; VanDerveer, D.; Williams, L. D. *Biochemistry* **2001**, *40* (34), 10023−10031.
(90) Cesare Marincola, F.; Denisov, V. P.; Halle, B. *J. Am. Chem. Soc.* **2004**, *126* (21), 6739−6750.
(91) Caceres, C.; Wright, G.; Gouyette, C.; Parkinson, G.; Subirana, J. A. *Nucl. Acids Res.* **2004**, *32* (3), 1097−102.
(92) Wong, A.; Wu, G. *J. Am. Chem. Soc.* **2003**, *125* (45), 13895−13905.

experiment reported and the first $^{1}H-^{205}Tl$ scalar coupling in a biological system.[80]

The techniques presented in this work can be readily extended to any system in which Tl^{+} can be substituted for K^{+}, resulting in a coordinated cation in slow exchange on the ^{205}Tl chemical shift time scale. One advantage of ^{205}Tl NMR is that its large chemical shift range provides a generous time scale for the slow exchange regime. If ^{1}H chemical shift assignments are available, the $^{1}H-^{205}Tl$ spin-echo difference experiment can be used to identify residues residing near the monovalent binding site(s). Information from this experiment could provide constraints for structure determination and allow monitoring of the response of monovalent cation sites to mutation or other perturbations. The relative simplicity of the difference spectrum means that this technique is feasible even when spectral overlap would be problematic in a one-dimensional ^{1}H spectrum. We anticipate the further development of $^{1}H-^{205}Tl$ NMR spectroscopy could prove useful for the study of monovalent cations and their binding sites in a variety of biological and inorganic systems.

Finally, the power of direct detection ^{205}Tl NMR is demonstrated by the observation of a previously unobserved complexity in the association of monovalent cations with the G-quadruplex system. The usefulness of the $^{1}H-^{205}Tl$ experiment is proven by the site-specific detection and assignment of bound $^{205}Tl^{+}$ ions with many additional applications foreseeable.

Acknowledgment. We thank Xiaoling Wu, Eric Paulson, Professor Kurt Zilm, Ben Bangerter, and Corey Morcombe for experimental assistance. Professor Melanie Cocco was instrumental in setting up the initial direct detection thallium experiment in the Department of Chemistry. We thank Jarislov Zajicek and Professor Thomas Nowak at the University of Notre Dame for access to their lower field instrument. We thank Prof. Victor Batista, Dr. Jose Gascon, and Christina Ragain for assistance with the quantum mechanics calculations. This research was supported by NIH R01 GM61249 to S.S. and J.P.L. M.L.G. acknowledges support from an NSF graduate fellowship.

JA055358F